Microwave bifurcation of a Josephson junction: Embedding-circuit requirements

V. E. Manucharyan, E. Boaknin, M. Metcalfe, R. Vijay, I. Siddiqi,* and M. Devoret
Department of Applied Physics, Yale University, New Haven, Connecticut 06511, USA
(Received 10 December 2006; revised manuscript received 21 February 2007; published 26 July 2007)

A Josephson tunnel junction which is rf driven near a dynamical bifurcation point can amplify quantum signals. However, the bifurcation point will exist robustly only if the electrodynamic environment of the junction meets certain criteria. We develop a general formalism for dealing with the nonlinear dynamics of a Josephson junction embedded in an arbitrary microwave circuit. We find sufficient conditions for the existence of the bifurcation regime: (a) the embedding impedance of the junction needs to present a resonance at a particular frequency ω_R, with the quality factor Q of the resonance and the participation ratio p of the junction satisfying $Qp \gg 1$, and (b) the drive frequency should be low frequency detuned away from ω_R by more than $\sqrt{3}\omega_R/(2Q)$.

DOI: 10.1103/PhysRevB.76.014524 PACS number(s): 85.25.Cp, 84.30.Le, 84.40.Az, 84.40.Dc

I. INTRODUCTION

Amplifying very small electrical signals is a ubiquitous task in experimental physics. In particular, cryogenic amplifiers working in the microwave domain found a growing number of applications in mesoscopic physics, astrophysics, and particle detector physics.[1,2] We have recently proposed[3,4] to use the dynamical bifurcation of a rf-biased Josephson junction (JJ) as a basis for the amplification of quantum signals. A bifurcation phenomenon offers the advantage of displaying a diverging susceptibility which can be exploited to maximize the amplifier gain without necessarily sacrifying its bandwidth. Among all very-low-noise and fast solid-state microwave devices, the Josephson junction distinguishes itself by offering strongest nonlinearity combined with weakest dissipation. However, these characteristics are not by themselves sufficient. The electrodynamic environment of the junction must also satisfy a certain number of conditions in order for a controllable and minimally noisy operation to be possible. In the recent Josephson bifurcation amplifier experiments,[3,4] the junction was shunted by a lumped element capacitor. A large capacitance had to be fabricated very close to the junction to minimize parasitic circuit elements, at the cost of severe complexity of patterning and thin-film deposition. It would be very beneficial experimentally to simply embed the Josephson junction in a planar superconducting microwave resonator. The aim of this article is to establish theoretically the requirements that need to be imposed on the embedding impedance of the junction in order to obtain a bifurcation whose characteristics are suitable for amplification.

The article is organized as follows: after having briefly indicated the connection between a bifurcating dynamical system and amplication, we review the simplest nonlinear dynamical system exhibiting the type of bifurcation we exploit: namely, the Duffing oscillator. We then describe the parameter space of the oscillator, focusing on the neighborhood of the first bifurcation and discussing why this is the most useful region. Having laid the general framework for the analysis of our problem, we then consider the simplest practical electrical implementation of the Duffing oscillator, a Josephson junction biased by an rf source through an arbitrary microwave circuit. The notion of embedding impedance is introduced. For concreteness, we first examine the particular cases where the embedding impedance corresponds to simple series or parallel LCR circuits. This allows us to formulate the conditions under which the resulting nonlinear electrical system can be mapped onto the Duffing model. We then examine the arbitrary impedance case, finding that it must correspond to that of a resonator with an adequate quality factor. We end the article by discussing possible detailed experimental implementations of resonators and a concluding summary.

II. AMPLIFYING WITH THE BIFURCATION OF A DRIVEN DYNAMICAL SYSTEM

Amplification using a laser, a maser, or a transistor is based on energizing many microscopic systems, like atoms in a cavity or conduction electrons in a channel, each one being weakly coupled to the input signal. The overall power gain of the system, which is determined by the product of the number of active microscopic systems and their individual response to the input parameter, can be quite substantial. However, noise can result from the lack of control of each individual microscopic system. This article explores another strategy[5] for amplification which involves a single system with only one very-well-controlled collective degree of freedom, which is driven to a high level of excitation. Here, the input signal is coupled parametrically to this system and influences its dynamics. The best known device exploiting this strategy is the superconducting quantum interference device[6] (SQUID) but other devices of the same type have been proposed.[7] Let us discuss the general question of the gain (ratio of output to input) in such a system.

A driven dynamical system such as a SQUID is governed by a force equation which, quite generally, can be written as

$$\mathcal{F}(\ddot{X},\dot{X},X,a) = F_{ext}(t), \tag{1}$$

where X is the system coordinate, $F_{ext}(t)$ is a periodic external drive pumping energy in the system, a a parameter of the system, and $\mathcal{F}$ a function describing its dynamics which is necessarily dissipative since information is flowing away to

the next stage of amplification. We are interested in a steady-state solution of Eq. (1), in which the energy flowing in from the source is balanced by the energy losses. In the example of the rf SQUID, X is the total flux through the SQUID loop, a the signal flux, and F the external driving flux with a frequency in the MHz range. For the dc SQUID,[9] the frequency of the external drive current is 0 and X is the common mode phase difference while a is the flux through the loop formed by the junctions. In this article we also consider a Josephson-junction-based device like a SQUID, but it is driven by a rf signal at microwave frequencies to increase speed and does not have intrinsic dissipation.

When we use the dynamical system as an amplifier, we are linking the input and output signals to the parameters a and variable X, respectively. Specifically, the signal $s(t)$ at the input of the amplifier induces a variation $\delta a = \lambda s$. For a small input, the output $S(t)$ of the amplifier will depend linearly on the modification of X: $S(t) = \mathcal{L}\{X(t) - X(t)_{s=0}\}$. Since we are looking for a maximal signal gain S/s, it is natural to find an operating point where a small change in the parameter a is going to induce a large change in the dynamics of the system, provided we can keep all other parameters constant. The largest differential susceptibility is found at a saddle-node bifurcation point, and it is in the neighborhood of such points that we will operate the amplifier. The saddle-node bifurcation occurs when the drive parameters exceed certain critical values. Previously, Yurke *et al.*[8] studied Josephson systems mostly in the regime beneath these critical values. Here, we consider similar systems, but we exploit instead the bistable regime *beyond* the critical values and the large susceptibilities accompanying it. In the next section, we review a simple model exhibiting such a saddle-node bifurcation phenomenon.

III. ONE MINIMAL MODEL FOR A BIFURCATING NONLINEAR SYSTEM: THE DUFFING OSCILLATOR

One of the most minimal models displaying the bifurcation phenomenon needed for amplification is a damped, driven mechanical oscillator with a restoring force displaying cubic nonlinearity. The equation of this model, often called the Duffing linear+cubic oscillator,[10–12] is

$$m\ddot{X} + \gamma\dot{X} + kX(1 - \nu X^2) = F\cos\omega_d t + F_N(t), \tag{2}$$

where X is the position coordinate of the mechanical degree of freedom, m its mass, γ its damping constant, k the stiffness constant of the restoring force, and ν the nonlinearity parameter. The right-hand-side parameters F and ω are the amplitude and angular frequency of the driving force, respectively. For completeness, we have also added on the right-hand side a noise force term $F_N(t)$ whose presence is imposed by the fluctuation-dissipation theorem. It defines, through its correlation function, a thermal energy scale for the problem, but in the following sections, we are going to assume that this scale can be made much smaller than all the other scales in the problem. The effect of fluctuations will be treated in a later article.

This simplification made, we can rescale the problem, changing the position and time coordinates, obtaining in the end a three-parameter model

$$\ddot{x} + \frac{\dot{x}}{Q} + x(1 - x^2) = f\cos w\tau, \tag{3}$$

where the dot now refers to differentiation with respect to the rescaled time τ. The following equations express the rescaled quantities in terms of the original ones: $\omega_0 = \frac{1}{\sqrt{m/k}}$, $\tau = \omega_0 t$, $w = \frac{\omega_d}{\omega_0}$, $Q = \frac{\sqrt{mk}}{\gamma}$, $x = \sqrt{\nu}X$, and $f = \frac{\sqrt{\nu}}{m}F$.

For reasons which will become clear later, we want to consider the low damping limit of such a model and we suppose that the quality factor satisfies $Q \gg 1$.

In the weak nonlinear regime—i.e., $x(\tau) \ll 1$–the frequency w_0 of natural oscillations ($f=0$) decreases with the oscillation energy $u = \frac{\dot{x}^2}{2} + \frac{x^2}{2} - \frac{x^4}{4}$ as

$$w_0 = 1 - \frac{3u}{2} + O(u^2). \tag{4}$$

This corresponds to the softening of the restoring force as the amplitude of the oscillatory motion increases.

The bifurcation phenomenon can be described crudely as follows: if we drive the system below the small oscillation resonance frequency, increasing the drive amplitude slowly, the resulting oscillation will be very small at first. However, at a certain drive strength, the system becomes unstable and tends to switch to a high amplitude oscillation where it can better meet the resonance condition.

In a quantitative treatment of the weak nonlinear regime, we seek a solution involving only the first harmonic of the drive frequency and make the following change of variables:

$$x(\tau) = \frac{1}{2}\tilde{x}(\tau)e^{iw\tau} + \frac{1}{2}\tilde{x}^*(\tau)e^{-iw\tau},$$

$$\dot{x}(\tau) = \frac{i\omega}{2}\tilde{x}(\tau)e^{iw\tau} - \frac{i\omega}{2}\tilde{x}^*(\tau)e^{-iw\tau}, \tag{5}$$

where the time dependence of the complex harmonic amplitudes $\tilde{x}(\tau)$ and $\tilde{x}^*(\tau)$ is slow on the time scale w^{-1}. Retaining in the equation only the terms evolving in time like $e^{iw\tau}$ one finds the following relation for $\tilde{x}(\tau)$ (Ref. 13):

$$2i\dot{\tilde{x}} = \left(\frac{\Omega - i}{Q} + \frac{3}{4}|\tilde{x}|^2\right)\tilde{x} + f, \tag{6}$$

in which we have introduced the reduced detuning Ω,

$$\Omega = 2Q(w - 1). \tag{7}$$

The static solutions ($\dot{\tilde{x}}=0$) for the modulus $\mathbf{x} = |\tilde{x}|$ of the fundamental amplitude can be obtained as a function of the parameters (Ω, f) for a given Q by solving the equation

$$f^2 = \left(\frac{\Omega^2 + 1}{Q^2} + \frac{3\Omega}{2Q}\mathbf{x}^2 + \frac{9}{16}\mathbf{x}^4\right)\mathbf{x}^2. \tag{8}$$

The differential susceptibility is given by the implicit expression

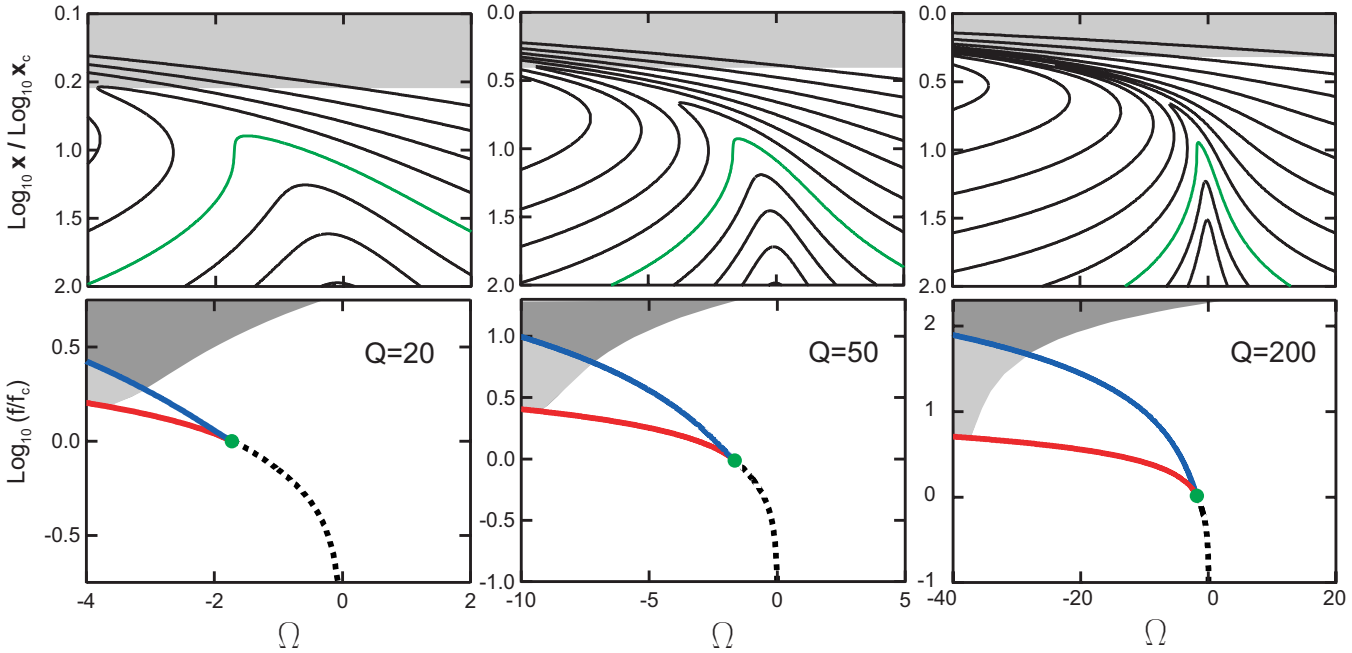

FIG. 1. (Color) *Upper panels:* response of the Duffing linear+cubic oscillator [see Eq. (2)] as a function of the dimensionless detuning Ω, for different values of the dimensionless driving amplitude f. The three panels correspond to three different values of the small oscillation quality factor $Q=20$, 50, and 200 and are shown over the same reduced frequency range $0.9<w<1.05$. The response for the critical drive amplitude f_c, where the curve presents a single point with diverging susceptibilities $\partial x/\partial\Omega$ and $\partial x/\partial f$, is shown in green. From bottom to top, the increments in the drive amplitude f are 2 dB (left), 2 dB (center), and 3 dB (right). In the gray region, the oscillation amplitude is taking place in the strongly nonlinear regime (see text) and the curves, which are calculated within the weak non-linear hypothesis, are not to be trusted. *Lower panels:* stability diagram for the dynamical states corresponding to the system response shown in the upper panels. The y axis is the drive amplitude f, scaled by the critical amplitude f_c. The blue $[f_B(\Omega)]$ and red $[f_{\bar{B}}(\Omega)]$ lines delimit the region of bistability for the system and correspond to the points of diverging susceptibility which are visible in the upper panels. The two curves meet at the critical point shown by a green dot, whose position is determined by the critical detuning $\Omega_c=-\sqrt{3}$ and drive amplitude f_c. The dashed line $[f_{ms}(\Omega)]$ "continues" the blue and red lines and corresponds to the points of maximal susceptibility with respect to driving force. The gray regions correspond to that in the upper panels. Note that the "trusworthy" domain of bistability increases monotonously with the quality factor Q.

$$\frac{\partial \mathbf{x}}{\partial f}=\left(\frac{\partial f}{\partial \mathbf{x}}\right)^{-1}=\frac{\sqrt{\frac{(1+\Omega^2)}{Q^2}+\frac{3\Omega}{2Q}\mathbf{x}^2+\frac{9}{16}\mathbf{x}^4}}{\frac{(1+\Omega^2)}{Q^2}+\frac{3\Omega}{Q}\mathbf{x}^2+\frac{27}{16}\mathbf{x}^4}. \tag{9}$$

In the upper panels of Fig. 1, we show $\mathbf{x}$ as a function of Ω for increasing values of f and for $Q=20,50,200$. For small drive, the curve is the familiar Lorentzian response of an harmonic oscillator, displaying a maximum response on resonance at $\Omega=0$ and a half width at half maximum (HWHM) point at $\Omega=-1$. As the drive strength is increased, the resonance curve bends towards lower frequencies, an indirect manifestation of Eq. (4). There is a critical drive f_c at which appears for the first time a critical reduced detuning Ω_c such that the susceptibility $\partial\mathbf{x}/\partial f$ diverges.[12] We call $\mathbf{x}_c$ the oscillation amplitude at this critical point. Analytic calculations[12,13] lead to

$$f_c=\frac{2^{5/2}}{3^{5/4}}\frac{1}{\sqrt{Q^3}},$$

$$\Omega_c=-\sqrt{3},$$

$$\mathbf{x}_c=\frac{2^{3/2}}{3^{3/4}}\frac{1}{\sqrt{Q}}. \tag{10}$$

To be consistent with our weak nonlinear regime hypothesis, we must have $\mathbf{x}_c\ll 1$ which implies in turn $Q\gg 1$.

For drives $f>f_c$, the response curve $\mathbf{x}(\Omega)$ develops an overhanging part in which there are three possible values for $\mathbf{x}$ at each value of Ω. The smallest and highest values correspond to two metastable states with different oscillation amplitudes, whereas the intermediate value corresponds to an unstable state for the system. We denote as $f_B(\Omega)$ and $f_{\bar{B}}(\Omega)$ the boundaries of this bistability interval: f_B is the force at which the system, submitted to an increasing drive with a fixed frequency, will switch from the low- to the high-amplitude state. Starting from this state and decreasing the amplitude of the oscillatory force, the system will switch back to the low-amplitude state at $f_{\bar{B}}$. This possibility of the Duffing system to "bifurcate" between two different dynamical states at $f_B(\Omega)$ and $f_{\bar{B}}(\Omega)$ is the phenomenon we are exploiting for amplification and whose electrical implementation is the main topic of this paper. It is easy to see that any input parameter coupled to k or m in Eq. (2) will induce variations of the line $f_B(\Omega)$. Fixing the drive parameters in

the vicinity of this line, very small changes in the input will induce large variations in the oscillation amplitude. The variations can be reversible if we chose a point to the right of the critical point (continuous amplifier operation) or the variations can be hysteretic if we chose a point to the left of the critical point (latched threshold detector operation).

In the limit $Q \gg 1$, analytic calculations can be carried further and lead to[13]

$$\frac{f_{B,\bar{B}}(\Omega)}{f_c} = \frac{1}{2}\frac{\Omega^{3/2}}{\Omega_c^{3/2}}\left[1 + 3\frac{\Omega_c^2}{\Omega^2} \pm \left(1 - \frac{\Omega_c^2}{\Omega^2}\right)^{3/2}\right]^{1/2}. \quad (11)$$

We define $f_{ms}(\Omega)$ as the line of maximum susceptibility $\partial \mathbf{x}/\partial f$ on the low-frequency side of the resonance curve. It defines the line of highest amplification gain below the bifurcation regime.[14] Its expression is given by

$$\frac{f_{ms}(\Omega)}{f_c} = \frac{3^{1/2}}{2}\frac{\Omega^{1/2}}{\Omega_c^{1/2}}\left[\frac{1}{3}\left(\frac{\Omega}{\Omega_c}\right)^2 + 1\right]^{1/2}. \quad (12)$$

The susceptibility on the high-frequency side of the critical point diverges as

$$\left.\frac{\partial \mathbf{x}}{\partial f}\right|_{\Omega \sim \Omega_c} = \frac{Q}{\Delta\Omega}, \quad (13)$$

where $\Delta\Omega$ is defined by $\Omega = \Omega_c - \Delta\Omega$ and $\Omega_c \gg \Delta\Omega$.

In the lower panels of Fig. 1, we plot the bifurcation forces f_B (blue line) and $f_{\bar{B}}$ (red line) and f_{ms} (dashed line) normalized to the critical force as a function of the reduced drive frequency Ω. Note that the lines representing $f_B(\Omega)$, $f_{\bar{B}}(\Omega)$, and f_{ms} in the parameter space $(\Omega, f/f_c)$ are independent of the parameters of Eq. (2) and can be deemed "universal."

The dynamical critical point $(\Omega = \Omega_c, f/f_c = 1)$ is found at the junction between the dashed line and the two bifurcation lines. One can develop an analogy between the parameter space $(\Omega, f/f_c)$ and the phase diagram of a fluid undergoing a liquid-vapor transition, the dynamical critical point corresponding to the critical point beyond which vapor and liquid cannot be distinguished by a transition (supercritical fluid regime) and the bifurcation lines corresponding to the limit of stability of the supercooled vapor and superheated fluid on either side of the first-order transition line (spinodal decomposition phenomenon).

A. Weak and strong nonlinear regimes for the simple Duffing equation

Let us now further discuss the small-amplitude condition $\mathbf{x} \ll 1$, which is necessary for the above results to hold. In the Appendix we show that as long as

$$\frac{3}{2w^2}\mathbf{x}^2 < \text{"few"}, \quad 1/2 < w < 1, \quad (14)$$

where "few" is a numerical constant difficult to determine but of order unity, the Duffing model has stationary solution of the form

$$x(\tau) = \frac{1}{2}\sum_{k=1}^{\infty}[\tilde{x}_{2k-1}e^{i(2k-1)w\tau} + \text{c.c.}], \quad (15)$$

with the coefficients $\tilde{x}_{2k-1}$ decreasing with the order k. Only odd multiples of the drive frequency thus appear in this series. The first harmonic coefficient $\tilde{x}_1$ is given by the stable solution of Eq. (6) in the limit $|\tilde{x}_1| \ll 1$. Inequalities (14) define the weak nonlinear regime.

By contrast, in the strong nonlinear regime $\frac{3}{2w^2}\mathbf{x}^2 >$ "few," even harmonics start to proliferate as the oscillation amplitude increases, leading eventually to chaotic behavior.[15–17] It is important to note that the SQUID does not avoid this regime, even if, in general, strong dissipation prevents fully developed chaos in this device.

Wanting at all cost to minimize noise in our use of this dynamical system for amplification, we want to avoid the strong nonlinear regime. Keeping in mind that we are going to work with a small detuning $(\omega - \omega_0)/\omega_0$, a conservative boundary separating the weak from the strong nonlinear regime can be introduced in parameter space by requiring

$$\mathbf{x} < 0.5. \quad (16)$$

In the lower panels of Fig. 1, the gray region corresponds to condition (16) being violated for at least one of the oscillation states. A lighter shade of gray marks the hysteretic region between $f_B(\Omega)$ and $f_{\bar{B}}(\Omega)$ to indicate that the low-amplitude state does not violate (16) while the high amplitude does.

Note that in the reduced parameter space $(\Omega, f/f_c)$, the line $f_{ms}(\Omega)$ corresponding to condition (16) has a rather drastic dependence on Q, in contrast with the other lines. Of course, if we would plot the stability boundary lines in the absolute parameter space (ω, F), the line corresponding to (16) would be fixed while the critical point (ω_c, F_c) would strongly depend on Q.

Whatever the representation, the important message which arises from the stability diagram is that the amount of "real estate" in parameter space that can be used for bifurcation amplification increases with Q. All points along the $f_B(\Omega)$ line located between f_c and $f_s(\Omega)$ are potentially useful. By realizing a large enough Q, one can always "buy" the necessary amount of "real estate" in the stability diagram, irrespectively of the value of the other parameters of the system. Of course, higher Q will tend to lower the bandwidth, but we can compensate this effect by increasing the operating frequency of the device.

IV. rf-BIASED JOSEPHSON JUNCTION

We now apply these general considerations to the practical case of a JJ biased by an rf source. At radio frequencies, the impedance of the biasing circuit cannot be taken either as zero (ideal voltage source) or infinite (ideal current source). In general, as depicted in Fig. 2(a), the biasing circuitry should be modeled as a specific, frequency-dependent linear quadrupole connecting the Josephson element of the junction to an ideal voltage source (the other circuit element of the junction, its linear capacitance, has been lumped in this

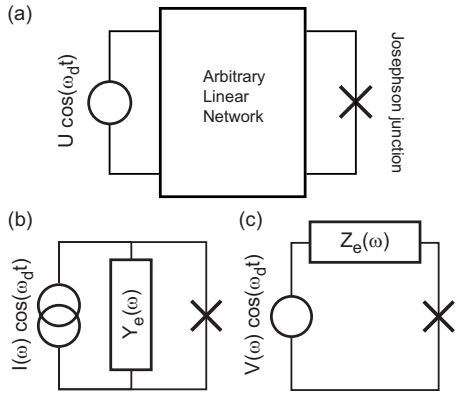

FIG. 2. (a) Schematic of a Josephson junction rf biased through an arbitrary electric quadrupole containing only linear components. The Thevenin (b) and Norton (c) representations of the circuit of (a) show the dipole seen by the junction. Note that the new source amplitude may now depend on frequency.

quadrupole). Taking the point of view of the junction and applying either the Norton or Thevenin representation, we arrive at the circuits of Figs. 2(b) and 2(c), respectively, where $Y_e(\omega)$ and $Z_e(\omega)$ are the admittance and impedance of the quadrupole seen from the junction. In this transformation of the problem, the amplitude of the source may now depend on frequency, but we ignore this complication for simplicity. It turns out that in the cases of interest, either the Norton or Thevenin (but not both) represention will satisfy this hypothesis adequately.

The Josephson electrical element, represented by a cross in our schematics, is defined by its constitutive equation

$$I(t) = I_0 \sin[\Phi_J(t)/\varphi_0] \tag{17}$$

involving the generalized flux defined by $\Phi_J = \int_{-\infty}^{t} V(t')dt$ (Ref. 18) and where $\varphi_0 = \hbar/2e$ is the reduced flux quantum. Here $V(t)$ and $I(t)$ are, respectively, the voltage across the junction and current through it.

Comparing Eq. (17) with the constitutive equation of an inductance,

$$I(t) = \frac{1}{L}\Phi(t), \tag{18}$$

we understand why the quantity

$$L_J = \left(\frac{\partial I}{\partial \Phi_J}\bigg|_{\Phi_J=0} \right)^{-1} = \varphi_0/I_0$$

is referred to as the effective Josephson inductance.

Note that Eq. (17) provides a nonlinear link between Φ_J and I and is, in some abstract sense, analogous to the relation between force and position for a nonlinear restoring force. However, the external circuit described by $Y_e(\omega)$ or $Z_e(\omega)$ also participates in the restoring force and we have to go through one further step in order to establish a link between our electrical system and the Duffing oscillator model.

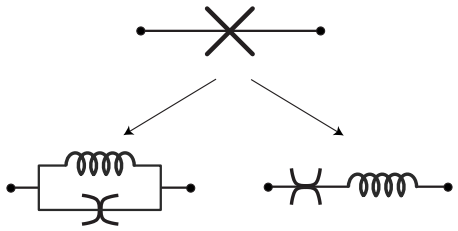

FIG. 3. Two possible ways of separating the linear and nonlinear contributions of a Josephson junction to a microwave circuit. Different symbols were chosen for the nonlinear elements to suggest their different current-voltage relations. The Josephson inductance in both cases has the usual value $L_J = \varphi_0/I_0$.

A. Separation of the linear and nonlinear contributions of the Josephson element

It is useful to split the Josephson element into its purely linear and nonlinear components. The linear contribution of the Josephson element is the impedance $iL_J\omega = Z_J(\omega)$ and can be incorporated in the biasing impedance. The nonlinear contribution, however, can be defined only by first referring to either the Norton or Thevenin representation.

We thus expand Eq. (17) in two different ways:

$$I(t) = \frac{1}{L_J}\Phi_J(t) - \frac{1}{6L_J\varphi_0^2}\Phi_J(t)^3 + O[\Phi_J^5(t)] \tag{19}$$

and

$$\Phi_J(t) = L_J I(t) + \frac{L_J^3}{6\varphi_0^2} I^3(t) + O[I^5(t)], \tag{20}$$

corresponding to these two representations, respectively. Relations (19) and (20) correspond, respectively, to a parallel and series combinations of a usual linear inductance of value L_J and a nonlinear element which is defined by the higher-order terms in the equations (see Fig. 3) and which is also characterized by the parameter L_J. We will call these nonconventional components *parallel* nonlinear (PNL) and *series* nonlinear (SNL) elements, respectively. They are represented by spider-like symbols in Fig. 3.

For the purpose of this paper, it will be sufficient to keep only the first nonlinear term in each of the expansions above. The cut-line spider symbol corresponds to the constitutive equation

$$I^p(t) = -\frac{1}{6L_J\varphi_0^2}\Phi_J(t)^3, \tag{21}$$

while the spine-line spider symbol corresponds to the constitutive equation

$$\Phi^s(t) = \frac{L_J^3}{6\varphi_0^2} I^3(t). \tag{22}$$

In the equation of our electrical system, these elements will lead to terms analogous to the nonlinear term in the Duffing equation (2).

Figure 4 shows the result of the complete transformation of the initial circuit, in which the linear part of the circuit is now described by the admittance $Y(\omega) = Y_e(\omega) + Z_J^{-1}(\omega)$ in the

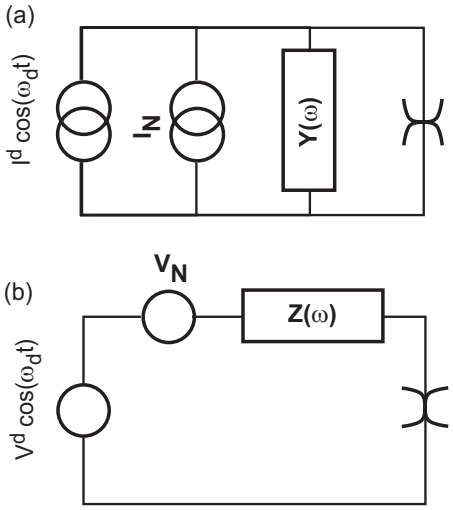

FIG. 4. Equivalent Norton (a) and Thevenin (b) representations of a linear circuit driving a PNL and SNL Josephson element, respectively. The appropriate bias source is shown as either a parallel current source or a series voltage source.

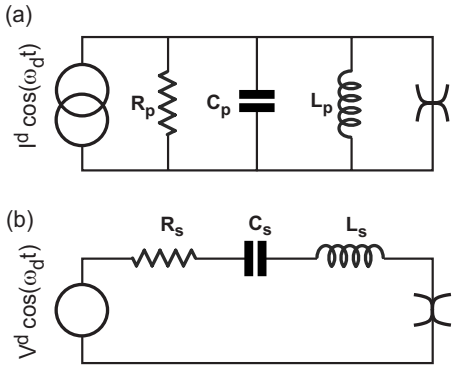

FIG. 5. Josephson junction biased by (a) a parallel *LCR* circuit and (b) a series *LCR* circuit. In the first case, $L_p^{-1}=L_{pe}^{-1}+L_J^{-1}$ and in the second case, $L_s=L_{se}+L_J$ where L_{pe} and L_{se} are the inductances contributed by the environment.

Norton case or by the impedance $Z(\omega)=Z_e(\omega)+Z_J(\omega)$ in the Thevenin case.

Much qualitative insight can be gained from Fig. 4(a). Indeed, it is clear that, in order to have the PNL element participate and induce a significant nonlinear behavior, one needs the current going through it to be large. For this to occur, the linear admittance $Y(\omega)$ must be small. This will occur in the vicinity of a resonance frequency of the linear part of the circuit: namely, when $\mathrm{Im}[Y(|\omega|)]=0$. The same reasoning applies for Thevenin representation [see Fig. 4(b)] where the voltage developed across the SNL element must be large—i.e., in the vicinity of a resonance where $\mathrm{Im}[Z(\omega)]=0$ holds.

B. Parallel and series *LCR* biasing circuits

We now consider the simplest cases where the environment of the nonlinear element—described by either $Y(\omega)$ or $Z(\omega)$—is either the parallel or series *LCR* circuit (see Fig. 5). These circuits are defined by the inductances, capacitances, and resistances L_p, C_p, and R_p in the parallel case and L_s, C_s, and R_s in the series case. From the discussion in the last section, L_p and L_s include the contribution of the Josephson effective inductance: for the parallel case, $L_p^{-1}=L_{pe}^{-1}+L_J^{-1}$, and for the series case, $L_s=L_{se}+L_J$, where L_{pe} and L_{se} are the inductances of the embedding circuit of the physical junction.

For the parallel case, the application of Kirchhoff's law to currents in all branches leads to the equation of motion

$$C_p\varphi_0\ddot{\delta}+\frac{\varphi_0}{R_p}\dot{\delta}+\frac{\varphi_0}{L_p}\delta\left(1-\frac{L_p}{6L_J}\delta^2\right)=I^d\cos\omega t, \qquad (23)$$

which is a strict analog of Eq. (2). Here we have introduced the so-called gauge-invariant phase difference $\delta=\Phi_J(t)/\varphi_0$. In Table I we show the correspondance between the mechanical system and this parallel *LCR* system. The associated critical parameters are given in Table II. Note that in this table the critical coordinates are referred to using the current $I_c=\delta_c I_0$. To a good approximation, this is the amplitude of

TABLE I. Table of correspondance between the parameters of the various realizations of the generalized Duffing equation [see Eq. (6)] considered in this article—i.e., the mechanical oscillator and the electrical oscillators based on a Josephson junction biased either through a parallel or a series *LCR* circuit. The notion of participation ratio p has meaning only in the case of the Josephson junction circuits in which the current through the junction cannot exceed its critical current.

Parameter	ω_0	Q	p	f	x
Mechanical	$\frac{1}{\sqrt{m/k}}$	$\frac{\sqrt{mk}}{\gamma}$	N.A.	$\frac{\sqrt{\nu}}{k}\mathrm{F}$	$\sqrt{\nu}X$
Parallel $J+LCR$	$\frac{1}{\sqrt{LC}}$	$R\sqrt{\frac{C}{L}}$	$\frac{L}{L_J}$	$\sqrt{\frac{L}{6L_J}}\frac{LI^d}{\varphi_0}$	$\sqrt{\frac{L}{6L_J}}\delta$
Series $J+LCR$	$\frac{1}{\sqrt{LC}}$	$\frac{1}{R}\sqrt{\frac{L}{C}}$	$\frac{L_J}{L}$	$\sqrt{\frac{L_J}{6L}}\frac{V^d}{L\omega_0 I_0}$	$\sqrt{\frac{L_J}{6L}}\frac{\omega_0}{I_0}q$

TABLE II. Values of system parameters (frequency, drive amplitude) and response (amplitude of oscillation) at the critical point for the various mechanical and electrical realizations of the Duffing system considered in this article. In the two boxes marked "implicit," the critical frequency can be obtained only by the solving the given equation.

	Parameters at the critical point		Response at the critical point
	Frequency	Drive amplitude	Oscillation amplitude
Mechanical	$\Omega_c \equiv 2Q\left(\frac{\omega_c}{\omega_0}-1\right)=-\sqrt{3}$	$f_c=\frac{2^{5/2}}{3^{5/4}}\frac{1}{\sqrt{Q^3}}$	$\mathbf{x}_c=\frac{2^{3/2}}{3^{3/4}}\frac{1}{\sqrt{Q}}$
Parallel $J+LCR$	$\Omega_c \equiv 2Q\left(\frac{\omega_c}{\omega_0}-1\right)=-\sqrt{3}$	$I_c^d=\frac{8}{3^{3/4}}\left(\frac{1}{Q}\frac{L_J}{L}\right)^{3/2}I_0$	$I_c \equiv \delta_c I_0=\frac{4}{3^{1/4}}\sqrt{\frac{1}{Q}\frac{L_J}{L}}I_0$
Series $J+LCR$	$\Omega_c \equiv 2Q\left(\frac{\omega_c}{\omega_0}-1\right)=-\sqrt{3}$	$V_c^d=\frac{8}{3^{3/4}}\left(\frac{1}{Q}\frac{L}{L_J}\right)^{3/2}\omega_c\varphi_0$	$I_c \equiv \omega_c q_c=\frac{4}{3^{1/4}}\sqrt{\frac{1}{Q}\frac{L}{L_J}}I_0$
Parallel $Y(\omega)$	$\frac{\mathrm{Im}[Y(\omega_c)]}{\mathrm{Re}[Y(\omega_c)]}=-\sqrt{3}$(implicit)	$I_c^d=\frac{8}{3^{3/4}}\left(\frac{\mathrm{Re}[Y(\omega_c)]}{\lvert Y_J(\omega_c)\rvert}\right)^{3/2}I_0$	$I_c=\frac{4}{3^{1/4}}\sqrt{\frac{\mathrm{Re}[Y(\omega_c)]}{\lvert Y_J(\omega_c)\rvert}}I_0$
Series $Z(\omega)$	$\frac{\mathrm{Im}[Z(\omega_c)]}{\mathrm{Re}[Z(\omega_c)]}=-\sqrt{3}$(implicit)	$V_c^d=\frac{8}{3^{3/4}}\left(\frac{\mathrm{Re}[Z(\omega_c)]}{\lvert Z_J(\omega_c)\rvert}\right)^{3/2}\omega_c\varphi_0$	$I_c=\frac{4}{3^{1/4}}\sqrt{\frac{\mathrm{Re}[Z(\omega_c)]}{\lvert Z_J(\omega_c)\rvert}}I_0$

the current through the junction at the critical point.

We now identify an important parameter which we call the parallel *participation ratio*:

$$p_p = L_p/L_J. \tag{24}$$

Together with the quality factor Q, it determines the ratio between the current I_{pc} at the dynamical critical point and the maximum Josephson supercurrent I_0 (see Table II). The participation ratio measures the strength of the nonlinearity: a small participation ratio is associated with a weak nonlinear term when $\delta \sim 1$ [see Eq. (23)].

We now turn to the case of the series *LCR* circuit shown in Fig. 5. Here, summing all the voltages across the elements of the circuit, we arrive at another equation of motion given by

$$L_s\ddot{q}\left(1+\frac{1}{2}\frac{L_J}{LI_0^2}\dot{q}^2\right)+R_s\dot{q}+q/C_s=V^d\cos\omega t, \tag{25}$$

where q is the total charge having flown through the junction up to time t. The cubic nonlinearity of this equation does not affect the restoring force like in the Duffing equation but the mass of the particle. Nevertheless, it is easy to show that the same Duffing oscillator dynamics is recovered at low drives within the single-harmonic approximation (see Table I). Like for the parallel case, the critical amplitude in Table II is given in a terms of a current $I_{sc}=\omega_c q_c$, which also here corresponds to the amplitude of the current through the junction at the critical point.

Again, we define the series *participation ratio*

$$p_s = L_J/L_s, \tag{26}$$

which plays the exact same role as p_p for the series case.

That the parallel and series cases can be mapped onto one another in the weak nonlinear regime (see Table I) is not an accident. Quite generally, one can show that any linear oscillator equation to which is added a cubic nonlinearity in any time-reversible combination of x and its derivatives ($\dot{x}$, $\ddot{x}$, etc.) will lead to, in the weak nonlinear regime, the same dynamics as that of Eq. (6). Non-time-reversible combinations would lead to a different type of (nondispersive) bifurcation which might be an interesting subject of investigation, but outside the scope of this paper.

The striking conclusion of this section on a lumped element resonator is that even when the junction has a weak participation ratio, its nonlinearity is not really "diluted." It will still display a bifurcation which can be employed for amplification, provided that the control of the amplitude of the oscillatory drive meets a corresponding increase in precision.

C. General biasing circuit involving a resonator

At the microwave frequencies where we wish to work, it is difficult to implement a pure *LCR* circuit without substantial parasitic elements. In practice, it will be easier to implement a distributed element resonator built with sections of transmission lines.[19,20] However, as we are going to demonstrate, the conclusions of the last section are robust provided that the quality factor of the resonator is chosen adequately, which is easily achievable with on-chip superconducting thin-film coplanar waveguides. We therefore now consider

the general case of an arbitrary impedance $Z(\omega)$ and use the Thevenin representation [see Fig. 4(b)]. The extension of our results to the case of an arbitrary admittance in the Norton representation will be straightforward, using the set of simultaneous transformation: $Z(\omega)\rightarrow Y(\omega)$, $Z_J(\omega)\rightarrow Y_J(\omega)$, SNL $\rightarrow$PNL.

We start by writing the equations of motion using Kirchoff's laws and make the variables change like in Eq. (5), $I(t)=\frac{1}{2}\tilde{I}(t)e^{i\omega t}+\text{c.c.}$ We now make three hypotheses: we first work within the rotating-wave approximation [i.e., $\tilde{I}(t)$ is assumed to be slowly varying on the scale of the drive period]; second, we assume that the impedance $Z(\omega)$ is a smooth function of frequency in the vicinity of the bifurcation region; finally, we neglect terms higher than cubic in the Josephson nonlinearity. Then one finds an equation of the form (6):

$$\sum_{n=1}^{\infty} i^n Z^{(n)}\tilde{I}^{(n)}(t)=\left(Z+\frac{1}{8}Z_J\left|\frac{\tilde{I}(t)}{I_0}\right|^2\right)\tilde{I}(t)-V_d. \qquad (27)$$

Here, $Z=Z(\omega=\omega_d)$, $Z_J=i\omega_d L_J$, $Z^{(n)}=\frac{d^nZ(\omega)}{d\omega^n}\big|_{\omega=\omega_d}$ are the derivatives of $Z(\omega)$ taken at the drive frequency, and $\tilde{I}^{(n)}=\frac{d^n I(t)}{dt^n}$. One can check that when $|\tilde{I}/I_0|\ll\sqrt{|Z/Z_J|}$—i.e., when nonlinearity can be neglected—the equation describes the complete response of the system. In particular, the steady-state oscillation amplitude is given by $\tilde{I}=V_d/Z(\omega)$. The zeros of $Z(\omega)$ are thus the complex resonant frequencies corresponding to the normal modes of excitations of the linear system (a well-built resonator has only a sparse set of zeros regularly distributed along the real frequency axis). The time derivative term on the left-hand side of Eq. (27) accounts for the transient dynamics.

The regime of interest for amplification is when $|\tilde{I}/I_0|$ approaches $\sqrt{|Z/Z_J|}$ for frequencies in the vicinity of a zero of $Z(\omega)$. We then find an equation bearing a close resemblance to Eq. (6) for the first harmonic of the Duffing oscillator amplitude. In the following, we will neglect all higher derivatives $Z^{(n>1)}$.

It is important to note that while Eq. (6) yields the bifurcation amplitude and drive as simple functions of the detuning frequency Ω, Eq. (27) only leads to the amplitude $\frac{\tilde{I}(t)}{I_0}$ and drives V_d at the bifurcation points as a function of the complex quantities Z and Z', which themselves have a smooth, but possibly complicated, dependence on ω_d. Although the expressions for generalized quantities such as $f_B(\Omega)$, $f_{\bar{B}}(\Omega)$, and $f_{ms}(\Omega)$ are tractable, they provide little insight. We therefore refrain from presenting them in this paper.

Nevertheless, we can still identify conditions that Z and Z' need to satisfy in order for the bifurcation real estate to exist. These conditions are obtained from Table II.

First, a critical drive frequency ω_c must exist such that the impedance $Z(\omega_c)$ satisfies the condition $\text{Re}[Z(\omega_c)]=-\sqrt{3}\,\text{Im}[Z(\omega_c)]$. A way to meet this condition is for the embedding impedance to have at least one resonant frequency ω_0 where $\text{Im}[Z(\omega_0)]=0$. Since for a passive circuit[21]

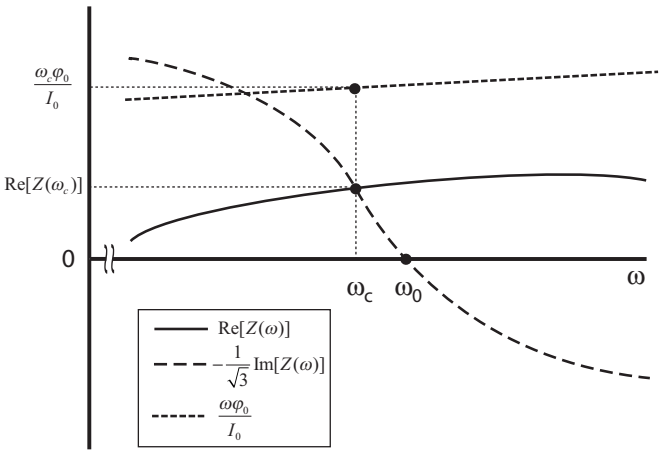

FIG. 6. Sketch of the graphical determination of whether a circuit characterized by impedance $Z(\omega)$ (see text) will allow a Josephson junction with critical current I_0 to bifurcate. The procedure consists in (i) plotting simultaneously $\text{Re}[Z(\omega)]$, $-\frac{1}{\sqrt{3}}\text{Im}[Z(\omega)]$ and $|Z_J(\omega)|=\omega\varphi_0/I_0$, (ii) finding the critical frequency ω_c (if it exists) at the eventual intersection $\text{Re}[Z(\omega)]=-\frac{1}{\sqrt{3}}\text{Im}[Z(\omega)]$, and (iii) verifying that the condition for weak nonlinearity is satisfied at ω_c: namely, $|Z_J(\omega_c)|\gg\text{Re}[Z(\omega_c)]$.

$$\left.\frac{d\,\text{Im}[Z(\omega)]}{d\omega}\right|_{\omega_0}=\text{Im}[Z'(\omega_0)]>0,$$

$$\text{Re}[Z(\omega_0)]>0, \qquad (28)$$

a critical frequency can be found at

$$\omega_c\simeq\omega_0-\frac{\text{Re}[Z(\omega_0)]}{\sqrt{3}\;\text{Im}[Z'(\omega_0)]+\text{Re}[Z'(\omega_0)]}, \qquad (29)$$

assuming the impedance is a smooth function of frequency near the resonant frequency. Equation (29) is useful from a practical point of view because it serves a guide in the generic case where the embedding impedance is not a simple oscillator. Although we have not proven it rigorously, we conjecture its validity in all cases of practical interest. In Fig. 6 we show how an exact solution for the frequency ω_c can be obtained graphically from a measurement of $\text{Im}[Z(\omega)]$ and $\text{Re}[Z(\omega)]$ in the neighborhood of ω_0. The graphical construction shows that the critical drive frequency needs to be located on the low-frequency flank of a resonance of the bias circuit, as in the case of the simple *LCR* circuit.

A second condition has to be fulfilled, however: the last line of Table II indicates that, at the critical frequency, the real part $\text{Re}[Z(\omega_c)]$ of the impedance must be much smaller than the effective impedance $\omega_c\varphi_0/I_0=L_J\omega_c$ of the junction. The ratio of the rf critical current I_c to the dc critical current I_0 must be much smaller than 1 in order to fulfill the condition of weak nonlinearity. The smaller the $\text{Re}[Z(\omega_c)]/|Z_J(\omega_c)|$ ratio, the larger becomes the "real estate" available for bistability in the stability diagram. This last consideration sets the maximum amount of dissipation which can be tolerated in the embedding impedance $Z_e(\omega)$.

It is useful to translate this last condition into a more practical language. If we introduce the generalized quality factor $Q(\omega)$ of the environmental impedance,

$$Q(\omega) = \frac{\mathrm{Re}[Z_{env}(\omega)]}{\omega\, \mathrm{Im}[Z'_{env}(\omega)]}, \tag{30}$$

we find that the condition on I_c can be rewritten as

$$\frac{8}{3^{1/4}} \sqrt{\frac{1}{Q(\omega_c)p}} < 1. \tag{31}$$

Thus, the higher the product of Q and p, the greater the real estate for amplification.

V. FURTHER DISCUSSION

The phenomenon of bistability has been recently observed in an electrical circuit biasing a Josephson junction.[4,22] Its operation as an amplifier has been studied[3] and used to measure a superconducting qubit.[23,24] The amplification near a bifurcation point is limited by a stochastic dynamical escape process similar to the one observed in dc biased JJs. This process is well studied theoretically in the classical regime where the fluctuations stem from thermal noise.[13,25] The quantum regime is not as well understood but important results can be found in Refs. 26 and 27. The circuit of Ref. 4 is based on the simplest realization of such an rf-biased junction: namely, a parallel *LCR* circuit. The resistance was provided by the 50-Ω rf environment, the capacitance was constructed lithographically on chip, and the inductance came entirely from the junction itself.

Another approach is to use continuous-circuit elements instead of discrete ones such as *L*'s, *R*'s, and *C*'s. A resonator structure with low internal loss can be used to bias the junction. Examples of these can range from a waveguide resonator, a lithographic resonator (see, e.g.,[20]), or any other resonator geometry. Any harmonic of such structure can be used to bias the JJ. The key lies in finding the correct way to couple the JJ. Let us discuss briefly a particular implementation: namely, using a coplanar waveguide cavity resonator such as the ones recently used to observe cQED in a solid-state system.[20] There, a junction can be placed at the center of the transmission line, interrupting its central conductor. The circuit analysis shows that this corresponds to the case discussed above of a JJ biased by a series *LCR* circuit. We have successfully fabricated and tested such devices and will discuss the results in a later paper.

VI. CONCLUDING SUMMARY

In this paper we have presented and discussed the idea of harnessing, for amplification purposes, the bifurcation phenomenon of a driven Josephson junction embedded in a resonating circuit. We first reviewed the basic mathematics associated with the general saddle-node bifurcation phenomenon using the simplest example of the mechanical Duffing oscillator. We then applied the corresponding formalism to a simple rf-driven *LCR* electrical oscillator incorporating a Josephson junction and found the conditions for observing bistability and a diverging susceptibility. There are two relevant parameters: the quality factor Q and the participation ratio. The latter quantity is necessarily smaller than unity and is a measure of the strength of the nonlinearity provided by the JJ, relative to the embedding circuit. We have found that the product of these two parameters need to be much greater than 1 in order to provide a convenient operating conditions for amplification. We then showned that the same condition applies to a more general resonating structure, with a simple adaptation of the definition of the quality factor and participation ratio to the vicinity of a resonance. Our prescription involves a relatively precise analysis of the microwave circuit of the resonator but can easily be followed with a varieties of geometries since microwave resonators can easily be made to have large quality factors. Later generations of amplifiers or detectors based on the bifurcation of superconducting resonators should therefore benefit from the analysis presented in this article.

ACKNOWLEDGMENTS

We would like to thank D. Esteve, D. Vion, R. Schoelkopf, and M. Dykman for useful discussions. This work was supported by NSA through ARO Grant No. W911NF-05-1-0365, the Keck Foundation, and the NSF through Grant No. DMR-0325580.

APPENDIX: WEAK AND STRONG NONLINEAR REGIMES FOR A NONLINEAR OSCILLATOR

In this appendix we would like to examine the behavior of a driven nonlinear oscillator beyond the simple framework developed in the main body of the paper which considers that the circuit only responds at the frequency of the driving force. We investigate the limits in which this hypothesis is violated, specializing to the realistic case of a Josephson junction. Our analysis relies heavily on the work developed in Refs. 10, 11, and 15–17. We will consider the generalization of Eq. (2) to an arbitrary nonlinear potential. To simplify the notation and to avoid confusion with the main text, we use $X \to y$, $m \to 1$, replace $\omega_d \to \omega$, and drop the noise term $F_N(t)$ from Eq. (2). The purely nonlinear force is written as $N(y)$, and we thus start with

$$\ddot{y} + \gamma\dot{y} + \omega_0^2 y + N(y) = f \cos \omega t. \tag{A1}$$

We will restrict our discussion to a nonlinear force $N(y)$ which is an antisymmetric function of y as this is the case relevant to the nonlinearity provided by a Josephson junction. It will also simplify the discussion.

A solution to Eq. (A1) can be found in the following form:

$$y(t) = y^{odd}(t,n) + \delta y(t,n), \tag{A2}$$

where the function $y^{odd}(t,n)$ is a sum of a finite number n of odd harmonics,

$$y^{odd}(t,n) = \frac{1}{2}\sum_{k=1}^{n} \tilde{y}_{2k-1} e^{i(2k-1)\omega t} + \text{c.c.}, \tag{A3}$$

while $\delta y(t,n)$ is a correction to the expansion. Note that n is introduced here as an integer-valued parameter.

By assuming $\delta y(t,n) \ll y^{odd}(t,n)$ we will conduct a linear analysis of this correction. Keeping $Q=\omega_0/\gamma$ constant [see Eq. (A1)], we find two different behaviors for $\delta y(t,n)$ depending on the parameters $\{\omega,f\}$ (their values are discussed later below):

(i) $\delta y(t,n)$ is bounded in time and contains only *odd* harmonics of ω starting with $2n+1$. It follows that Eq. (A3) is a good approximation for the stationary solution of Eq. (A1). The choice of n is determined by the required accuracy of the solution. The amplitudes of the stationary oscillations $\tilde{y}_k$ are functions of the drive frequency ω and amplitude f given by a system of nonlinear *algebraic* equations in terms of $N(y)$.

(ii) $\delta y(t,n)$ is unbounded in time. This would lead to the breakdown of the validity of our linear analysis or is, at least, an indication that the form for the solution given in Eq. (A3) has to be modified. The instability of $\delta y(t,n)$ can be of two types:

(iia) $\delta y(t,n) \sim e^{\lambda t} e^{i\omega(2k-1)t}$, where $k \leqslant n$ is an integer and $\lambda > 0$ is a Lyapunov exponent. The instability of this type corresponds to the switching of the oscillation amplitude from one stationary state to another at frequency $(2k-1)\omega$. This instability is of major interest to us as a resource for amplification purposes. In particular, for $k=1$, a switching between two stable states can occur.

(iib) $\delta y(t,n) \sim e^{\lambda t} e^{i2k\omega t}$, $k \leqslant n$ is an integer. This is a different instability phenomenon because the solution contains growing *even* harmonics which breaks the symmetry of the nonlinearity $N(-y)=-N(y)$. It was shown to be a precursor of chaotic behavior of a nonlinear oscillator, at least for the Duffing case, where $N(y) \propto y^3$.

Let us fix n and write down the system of nonlinear algebraic equations that defines $\tilde{y}_k$, $k=1,2,\ldots,n$ by using the harmonic balance method:

$$\tilde{y}_{2k-1}[1-(2k-1)^2\omega^2 + i(2k-1)\omega\gamma] + \tilde{N}^n_{2k-1}(\tilde{y}_1,\ldots,\tilde{y}_{2n-1}) = \frac{f}{2}\delta_{1,2k-1}, \tag{A4}$$

where $\delta_{1,2k-1}$ is the Kronecker delta function. The complex functions $\tilde{N}^n_{2m-1}(z_1,z_3,\ldots,z_{2n-1})$ are defined as

$$\tilde{N}^n_{2m-1}(z_1,\ldots,z_{2n-1}) = \int_{-\pi}^{\pi} N\left(\frac{1}{2}\sum_{k=1}^{n} z_{2k-1}e^{i(2k-1)\theta} + \text{c.c.}\right) \times e^{-i(2m-1)\theta}\frac{d\theta}{2\pi}. \tag{A5}$$

The solution of Eq. (A4) gives the amplitudes $\tilde{y}_{2k-1}(f,\omega)$ as a function of drive amplitude and frequency. Note that only the $k=1$ harmonic is driven directly by an external force, while the higher harmonics feel the drive via the nonlinearity.

The correction $\delta y(t,n)$ is obtained by subtracting the solutions to $y^{odd}(t,n)$ [see Eq. (A4)] from the solution of the initial equation [Eq. (A1)] and keeping the linear terms in δy. This leads to

$$\delta\ddot{y}(t,n) + \gamma\delta\dot{y}(t,n) + \omega_0^2\delta y(t,n) + N'(y^{odd}(t,n))\,\delta y(t,n) = h(y^{odd}(t,n)). \tag{A6}$$

Here $N'(y)=\frac{dN(y)}{dy}$.

One can see that the correction $\delta y(t,n)$ obeys the equation of a harmonic oscillator driven with a force $h(y^{odd}(t,n))$ and parametrically driven with $N(y^{odd}(t,n))$. The force $h(y^{odd}(t,n))$ is defined by

$$h(y^{odd}(t,n)) = \sum_{k=n+1}^{\infty} \tilde{N}^n_{2k-1}(\tilde{y}_1,\ldots,\tilde{y}_{2n-1})e^{i(2k-1)\omega\tau} + \text{c.c.}, \tag{A7}$$

where "c.c." is the complex conjugate. Note that $h(y^{odd}(t,n))$ contains only odd harmonics starting from $2n+1$. If the oscillator is parametrically stable, the correction $\delta y(t,n)$ will only contain oscillations at higher odd harmonics. They can be taken into account in principle by increasing the number of odd harmonics n in Eq. (A3). This means that we can ignore the drive term for the analysis of parametric instabilities. The stability analysis will now be reduced to the analysis of the parametrically driven harmonic oscillator which is very well understood.

Because the function $N'(y)$ is even, $N'(y^{odd}(\tau,n))$ contains only *even* harmonics of ω. That is,

$$N'(y^{odd}(\tau,n)) = \frac{1}{2}\sum_{k=0}^{\infty} \tilde{N'}^n_{2k}(\tilde{y}_1,\ldots,\tilde{y}_{2n-1})e^{i2k\omega t} + \text{c.c.}, \tag{A8}$$

with Fourier amplitudes $\tilde{N'}^n_{2k}$ given by

$$\tilde{N'}^n_{2m}(z_1,\ldots,z_{2n-1}) = \int_{-\pi}^{\pi} N'\left(\frac{1}{2}\sum_{k=1}^{n} z_{2k-1}e^{i(2k-1)\theta} + \text{c.c.}\right) \times e^{-i2m\theta}\frac{d\theta}{\pi}. \tag{A9}$$

Now the equation for the parametric driven correction δy can be rewritten in the form

$$\delta\ddot{y}(t,n) + \gamma\delta\dot{y}(t,n) + \delta y(t,n) \times\left(1 + \tilde{N'}^n_0 + \sum_{k=1}^{\infty}[\tilde{N'}^n_{2k}(\tilde{y}_1,\ldots,\tilde{y}_{2n-1})e^{i2k\omega t} + \text{c.c.}]\right) = 0. \tag{A10}$$

Equation (A10) is known in the literature on differential equations as Hill's equation with linear damping. Methods to investigate its stability diagram both analytically and numerically can be found in Ref. 11, for example.

The goal of our discussion can be achieved by considering the simplest form of Eq. (A10). We will take $n=1$ corresponding to the single-mode solution $y^{odd}(t,1) \equiv y_1(t) = \frac{1}{2}(\tilde{y}_1 e^{i\omega t} + \text{c.c.})$ and truncate the series (A8) to only the first and second terms. This corresponds to a dc shift in the linear oscillation frequency and to the 2ω parametric drive with amplitude $\tilde{N'}^1_2(\tilde{y}_1)$. This approximation is rich enough to un-

derstand the bistability of the first-harmonic response of a driven nonlinear oscillator as discussed in the main body of the paper. It also shows the roads that lead to the breakdown of the simple picture of bistability. These simplifications lead to

$$\delta\ddot{y} + \gamma\delta\dot{y} + \delta y\{\omega_0^2 + \tilde{N'}_0^1(\tilde{y}_1) + |\tilde{N'}_2^1(\tilde{y}_1)|\cos(2\omega t + \mathrm{Arg}[\tilde{N'}_2^1])\} = 0, \tag{A11}$$

where we have simplified our notation by using $\delta y(t,1) \equiv \delta y$. To reach the canonical form let us shift and rescale time by defining $2t' \equiv 2\omega t + \mathrm{Arg}[\tilde{N'}_2^1]$ and introduce two parameters of central importance:

$$\alpha = \frac{\omega_0^2 + \tilde{N'}_0^1}{\omega^2}, \quad \beta = \frac{|\tilde{N'}_2^1|}{\omega^2}, \tag{A12}$$

where $\tilde{N'}$ is evaluated at $\tilde{y}_1$. We get

$$\delta\ddot{y} + \frac{1}{Q}\delta y + (\alpha + \beta\cos 2t')\delta y = 0. \tag{A13}$$

This is known as Mathieu's equation with damping.[11] The main instability region corresponds to *order-1 parametric resonance*. It can be intuitively understood as a result of the efficient pumping of an oscillator at frequency $\sqrt{\alpha} \sim 1$. This instability leads to growing oscillations of $\delta y \sim e^{\lambda' t'} e^{it'} = e^{\lambda\tau} e^{i\omega t}$. Importantly, they are at *the same frequency as our odd anzatz* $y^{odd}(t,1)$. This can be incorporated into the anzatz by replacing $\tilde{y}_1 \to \tilde{y}_1(t)$. This was done in the main body of the paper and was shown to lead to hysteresis and bistability. In terms of $\alpha(\omega,\tilde{y}_1)$ and $\beta(\omega,\tilde{y}_1)$ the unstable (bistable) region is given by

$$\alpha(\omega,\tilde{y}_1) = 1 \pm \sqrt{\frac{\beta(\omega,\tilde{y}_1)^2}{4} - \frac{1}{Q^2}} - \frac{\beta(\omega,\tilde{y}_1)^2}{32}. \tag{A14}$$

The two nearest instabilities of the "wrong" type correspond to a second-order parametric resonance when $\sqrt{\alpha} \approx 2$ and to the phenomenon of the drive-mediated negative restoring force when $\alpha < 0$. These two instabilities contain growing double-frequency and zero-frequency components in $\delta y(t)$, respectively, and they break the symmetry of the nondriven problem. The locus of these transitions, with an accuracy of order $o(|\beta(\omega,\tilde{y}_1)|^2)$, is given, respectively, by

$$\alpha(\omega,\tilde{y}_1) = 4 + \frac{1}{24}\beta(\omega,\tilde{y}_1)^2 \pm \sqrt{\frac{\beta(\omega,\tilde{y}_1)^2}{128} - \frac{4}{Q^2}} \tag{A15}$$

and

$$\alpha(\omega,\tilde{y}_1) = -\frac{1}{8}\beta(\omega,\tilde{y}_1)^2. \tag{A16}$$

For the Duffing potential, where $N(y) = \omega_0^2 y^3$, we found that α and β have a particularly simple form $\alpha^D = \frac{\omega_0^2}{\omega^2}(1 - \frac{3}{2}\tilde{y}_1^2)$ and $\beta^D = -\frac{\omega_0^2}{\omega^2}\frac{3}{2}\tilde{y}_1^2$.

We now arrive at the main result of this appendix: provided that $|\beta^D| = \frac{\omega_0^2}{\omega^2}\frac{3}{2}\tilde{y}_1^2 < 1$ and $1/2 < w = \omega/\omega_0 < 1$ the symmetry-breaking unstable regimes are inaccessible since neither Eqs. (A15) nor (A16) has a solution. The analysis conducted in this appendix provides the ground for discussing the nonlinear oscillator only in terms of a single-frequency oscillating response. We saw in the main body of the paper how this leads to a simple picture of bistability. The exact boundary at which this picture breaks down requires a sophisticated analysis. However, a simple analysis reveals that the instability regions are well separated from our region of interest for the relevant experimental parameters ($1 - w \sim 1/Q \ll 1$, $|\tilde{y}_1| \sim 1/\sqrt{Q} \ll 1$). More importantly, it shows that the breakdown of the simple bifurcation picture is Q independent in the limit of high Q and the size of the accessible bistability region can therefore be under control.

In conclusion, basing our work on Refs. 10, 11, and 15–17, we have explained that instabilities of the steady-state response of a Josephson junction nonlinear oscillator can be viewed as parametric resonances. This mapping allows us to classify the different instabilities and separate the ones of interest for bifurcation amplification from the unwanted ones displaying chaos. A "sound" bifurcation is garanteed when (i) the quality factor is much greater than unity, (ii) the relative detuning is of the order of the inverse of the quality factor, and (iii) the dimensionless oscillation amplitude is of order of the inverse of the square of the quality factor.

*Present address: Department of Physics, University of California, Berkeley, CA 94720, USA.

[1] N. Wadefalk, A. Mellberg, I. Angelov, M. E. Barsky, S. Bui, E. Choumas, R. W. Grundbacher, E. L. Kollberg, R. Lai, N. Rorsman, P. Starski, J. Stenarson, D. C. Streit, H. Zirath *et al.*, IEEE Trans. Microwave Theory Tech. **51**, 1705 (2003); N. Oukhanski, M. Grajcar, E. Il'ichev, and H.-G. Meyer, Rev. Sci. Instrum. **74**, 1145 (2003).

[2] R. Bradley, J. Clarke, D. Kinion, L. Rosenberg, K. van Bibber, S. Matsuki, M. Mück, and P. Sikivie, Rev. Mod. Phys. **75**, 777 (2003).

[3] I. Siddiqi, R. Vijay, F. Pierre, C. M. Wilson, M. Metcalfe, C. Rigetti, L. Frunzio, and M. H. Devoret, Phys. Rev. Lett. **93**, 207002 (2004).

[4] I. Siddiqi, R. Vijay, F. Pierre, C. M. Wilson, L. Frunzio, M. Metcalfe, C. Rigetti, R. J. Schoelkopf, M. H. Devoret, D. Vion, and D. Esteve, Phys. Rev. Lett. **94**, 027005 (2005).

[5] K. Wiesenfeld and B. McNamara, Phys. Rev. Lett. **55**, 13 (1985); Phys. Rev. A **33**, 629 (1986).

[6] M. Mück, C. Welzel, and J. Clarke, Appl. Phys. Lett. **82**, 3266 (2003).

[7] R. J. Schoelkopf, P. Wahlgren, A. A. Kozhevnikov, P. Delsing, and D. E. Prober, Science **280**, 1238 (1998).

[8] B. Yurke, L. R. Corruccini, P. G. Kaminsky, L. W. Rupp, A. D.

Smith, A. H. Silver, R. W. Simon, and E. A. Whittaker, Phys. Rev. A **39**, 2519 (1989).
[9] L. D. Jackel and R. A. Buhrman, J. Low Temp. Phys. **19**, 210 (1974).
[10] N. N. Boglyubov and Y. A. Mitropolskii, *Asymptotic Methods of the Theory of Non-linear Oscillations* (Gordon and Breach, New York, 1961).
[11] A. H. Nayfeh and D. T. Mook, *Nonlinear Oscillations* (Wiley, New York, 1979).
[12] L. D. Landau and E. M. Lifshitz, *Mechanics* (Pergamon, Oxford, 1969).
[13] M. I. Dykman and M. A. Krivoglaz, Physica A **104**, 480 (1980).
[14] In some instances, it may be more relevant to look at the maximum susceptibility $\partial \mathbf{x}/\partial\Omega$ with respect to Ω. For a positive susceptibility (on the low-frequency side), we can define a similar line f_{ms}^{Ω}. It is given by $\frac{f_{ms}(\Omega)}{f_c}=\frac{1}{\sqrt{2}}\left(3\frac{\Omega}{\Omega_c}-1\right)^{1/2}$.
[15] Y. H. Kao, J. C. Huang, and Y. S. Gou, Phys. Lett. A **131**, 92 (1988).
[16] S. Novak and R. G. Frehlich, Phys. Rev. A **26**, 3660 (1982).
[17] B. A. Huberman and J. P. Crutchfield, Phys. Rev. Lett. **43**, 1743 (1979).
[18] B. D. Josephson, Rev. Mod. Phys. **36**, 216 (1964).
[19] P. K. Day, H. G. LeDuc, B. A. Mazin, A. Vayonakis, and J. Zmuidzinas, Nature (London) **425**, 817 (2003).
[20] A. Wallraff, D. I. Schuster, A. Blais, L. Frunzio, R.-S. Huang, J. Majer, S. Kumar, S. M. Girvin, and R. J. Schoelkopf, Nature (London) **431**, 162 (2004).
[21] D. M. Pozar, *Microwave Engineering* (Wiley, Hoboken, NJ, 2005).
[22] J. C. Lee, W. D. Oliver, T. P. Orlando, and K. K. Berggren, IEEE Trans. Appl. Supercond. **15**, 841 (2005).
[23] I. Siddiqi, R. Vijay, M. Metcalfe, E. Boaknin, L. Frunzio, R. J. Schoelkopf, and M. H. Devoret, Phys. Rev. B **73**, 054510 (2006).
[24] A. Lupascu, E. F. C. Driessen, L. Roschier, C. J. P. M. Harmans, and J. E. Mooij, Phys. Rev. Lett. **96**, 127003 (2006).
[25] M. I. Dykman and M. A. Krivoglaz, Zh. Eksp. Teor. Fiz. **77**, 60 (1979).
[26] M. I. Dykman and V. N. Smelyanskii, Zh. Eksp. Teor. Fiz. **94**, 61 (1988).
[27] M. I. Dykman, Phys. Rev. E **75**, 011101 (2007).